Desalination and Water Treatment
www.deswater.com

doi: 10.5004/dwt.2021.26577

226 (2021) 147–156
June

Ultrasonic supported deletion of Rhodamine B on ultrasonically synthesized zinc hydroxide nanoparticles on activated carbon concocted from wood of cherry tree: experimental design methodology and artificial neural network

Masoumeh Kiani[a,*], Saideh Bagheri[a,*], Akram Khalaji[b], Nima Karachi[c]

[a]*Department of Chemistry, Payam Noor University, P.O. Box: 19395-3697, Tehran, Iran, emails: M.Kiani@pnu.ac.ir (M. Kiani), S_bagheri2010@yahoo.com (S. Bagheri)*
[b]*Department of Chemical Engineering, Amir Kabir University of Technology, P.O. Box: 64540, Tehran, Iran, email: Akramkhalaji70@gmail.com (A. Khalaji)*
[c]*Department of Chemistry, Marvdasht Branch, Islamic Azad University, Marvdasht, Iran, email: nimakarachi@miau.ac.ir (N. Karachi)*

Received 17 April 2020; Accepted 11 September 2020

ABSTRACT

Ultrasound-supported dispersive solid-phase micro-extraction based on nano sorbent videlicet zinc hydroxide nanoparticles loaded on activated carbon ($Zn(OH)_2$-NPs-AC) in combination with derivative spectrophotometry method for deletion of Rhodamine B dye in industrial wastewater using response surface methodology (RSM) was the focus of the present article. Through the instrumentality of artificial neural network (ANN) and RSM, influential parameters were determined and optimized. Initial dye concentration (mg L^{-1}), and amount of sorbent (mg), pH, and sonication time (min) as effective variables on the deletion of dye were closely examined. Initial RHB concentration of 26.5 mg L^{-1}, $Zn(OH)_2$-NPs-AC amount of 0.025 g, ultrasonication time of 4 min, and pH of 4.0 provided us with the perfect removal percentages (>100.0%). The analysis of variance and estimation of the correlation coefficient corroborated the reliability of the equation obtained by RSM considering both the predicted and experimental values of ultrasound-supported deletion of the analytes. The experimental and prognosticated values were in sound conformity. The thriving application of feed-forward neural network with a topology optimized by response surface methodology in the prediction of ultrasound-supported deletion of RHB dye by $Zn(OH)_2$-NPs-AC in this study, paved the way for further investigations. For ANN modeling, the number of hidden neurons, R^2, MSE, the number of epochs, and error histograms were decided on. Afterwards, for fitting a model to the experimental data, Temkin, Langmuir, D–R isotherm, and Freundlich models were employed. A proper description of the isotherm data by Langmuir model with the highest adsorption capacity of 76.38 mg g^1 for RHB was reported. The maximum RHB adsorption based on kinetic studies at the desired condition was shown to be obtainable within 4 min of the onset of nearly all experiments. In describing the experimental data of ultrasound-supported deletion of RHB at desired condition procured from RSM, simultaneous use of intraparticle diffusion model and pseudo-second-order rate equation was proven to be advantageous.

Keywords: Kinetic and isotherm; Artificial neural network; Cherry tree; Zinc hydroxide nanoparticles; Rhodamine B; Response surface methodology

* Corresponding authors.

1. Introduction

In many manufacturing processes of plastic, fabric, leather, paper, guest-host liquid crystal displays, food, mineral, and solar cells, hues are used. Therefore, finding organic dyes in wastes discharged from leather, paper, food, textiles, plastics, and cosmetic industries is not a new issue at all. Slow degradation, chemical stability, high toxicity, and carcinogenicity of dyes in industrial wastewater have drawn the attention of researchers in health care as well as researchers in environmental care [1–3]. Nowadays, environmental researchers and conservationists are concerned about the hazardous impacts of effluents containing hues and pigments [4]. These dyes (synthetic) are biologically inert materials and the presence of sunlight can change them from bioinert to biodegradable. Consequently, developing successful techniques to delete dyes to a value lower than the threshold limit was included in the working agenda of researchers [5,6]. Rhodamine-B (RHB, Fig. 1) dye has been considered as a potent stimulant for allergies, and its carcinogenicity after decomposition has drawn the attention. After being exposed to it, people complained of burning eyes, burning/pruritic skin, and pain in eyes and skin [7]. In inhalation of Rhodamine-B, respiratory complications including nasal burning, chest pain/tightness, dyspnea, cough, burning of the throat, and burning chest. If ingested, gastrointestinal complications might develop. That's why proper treatment of dyes effluent for eliminating colors before their discharge is of critical importance. Therefore, rapid and quantitative deletion of them due to their hazardousness and limitations was considered. The most conventional protocols are: coagulation, flocculation, membrane filtration, biosorption, electrochemical techniques, and adsorption [8–12]. Amongst above-mentioned protocols, adsorption was preferred as a simple and highly efficient method that can guarantee ease of operation, high capacity, and large scale ability with renewable adsorbents [13–15]. The privilege of being a real solvent-free technique was assigned to ultrasound-supported dispersive-solid-phase micro-extraction (UADSPME) [16,17] since in UA-DSPME via ensuing proper selection of extraction phase, selective and efficient extraction can simply be achieved and it is also considered as a green protocol due to deletion of organic solvents [18]. Excellent adsorption capacity and porosity as well as the surface area of activated carbon (AC) put this material at the forefront of absorbing heavy metals ions. In addition, AC in combination with other materials can be used to increase the adsorption capacity and can provide a more convenient setting to eliminate the adsorbent after the adsorption process [19]. The proper sample preparation steps in complete deletion of organic solvents minimized waste production which proved the great potentiality of the method for quantification of intended analytes in pretty small samples which again could confirm the convenient dimensions of the UADSPME system [20,21]. The quantity of extracted analyte was directly dependent on both concentrations of the analyte in the matrix and sample volume [22,23]. Any increase in the volume and concentration of the analyte existed in water, ambient air, production stream, etc., could result in a boost in the extraction efficiency via time [16,24–26]. Strong interest in nano-structure based sorbents for the pre-concentration of trace elements and noxious dyes is on the basis of their stronger efficiency and more number of reactive atoms [27]. The uniform dispersion of nano-structure sorbents in the extraction media assists prompt isolation and/or pre-concentration of analytes from the initial solution [28].

Furthermore, the recyclability advantage of some nano-sorbents after a simple washing stage adds to their potentiality [29]. The focal point of the current article is about scrutinizing the modification of the surface of activated carbon concocted from the wood of cherry tree utilizing zinc hydroxide nanoparticles by ultrasound synthesis and its subsequent usage in the ultrasound-supported deletion of Rhodamine B (RHB). Equilibrium and kinetic surveys were carried out applying concocted NP modified adsorbent. For modeling and optimization of experimental data, artificial neural network (ANN) and RSM (response surface methodology) were employed.

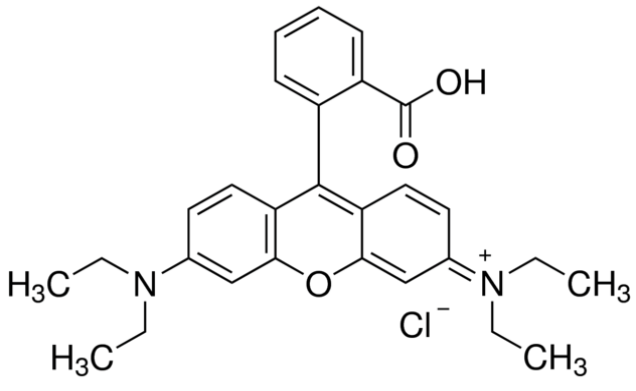

Fig. 1. Chemical structure of RHB.

2. Materials and method

2.1. Materials and characterization

Sigma Aldrich Company provided us with Zn $(CH_3COOH)_2$, HNO_3, NaOH, and HCl. From Merck (Darmstadt, Germany), Rhodamine B (RHB) was bought and it was utilized as received without additional purification. The concoction of 20 mg of RHB with 100 mL (200 mg L^{-1}) DW (distilled water) provided us the stock solution. Via proper dilutions of the stock solution with DW (distilled water), every single working solution was prepared. During the synthesis of $Zn(OH)_2$ nanoparticles for ultrasonic irradiation. With the help of a field emission scanning electron microscope (FESEM, Hitachi S4160, Japan), all the scanning electron images analysis were done. Also through the instrumentality of a spectrophotometer (Perkin Elmer spectrum RX-IFTIR), FTIR spectra of the activated carbon and $Zn(OH)_2$ nanoparticles loaded on activated carbon were procured over the 4,000–400 cm^{-1} range. The recording of X-ray diffraction (XRD, PW 1800 of Phillips Company Ltd., Holland) patterns from 10° to 100° was done utilizing CuKa as the X-ray source (k = 1.54 Å). For the ultrasound-supported adsorption experiments, an ultrasonic bath equipped with a heating and a degassing system (TECNO-GAZ, 60 Hz, 130 W, Parma, Italy) at 40 kHz frequency and 130 W power was exercised.

All the characterization applied in this article for the adsorbent prepared were fully described in our previous publication [30].

2.2. Apparatus

For registering the visible spectra and absorbance measurements (λ_{max} = 554 nm), an ultraviolet visible (UV-vis) spectrophotometer (model Pharmacia Ultraspec4000) with a 1 cm quartz cell equipment, was also employed. The XRD measurements were carried out on an XRD Bruker D8Advance. On a Shimadzu Fourier transform infrared (FTIR) 8000 spectrometer, the FTIR spectra were registered. For the pH measurement, a pH meter (Metrohm model-728) was adjusted. An ultrasonic homogenizer (UHP-400) (the product of Ultrasonic Technology Development Company, Iran) was utilized for the ultrasound-supported adsorption. All measurements were carried out at ambient temperature.

2.3. Statistical analysis

The software of STATISTICA 10.0 (State-Ease Inc., Minneapolis, USA) was employed to investigate about the experimental outcomes of the central composite design (CCD). Also for modeling and optimizing the impacts of concentration of initial RHB concentration (X_1), PH (X_2), amount of adsorbent (X_3), and contact time (X_4) on the ultrasonic-supported adsorption of RHB by $Zn(OH)_2$NPs-AC, RSM was employed. In Tables 1 and 2, the R% of RHB for four independent variables which were adjusted at five levels is shown. In order to assess the main and efficient terms for modeling the response on the basis of F-test and p-values, ANOVA or the analysis of variance was exercised [31].

2.4. Batch sorption experiments

As a means to evaluate the impact of adsorbent mass, pH, sonication time, and initial RHB concentration under RSM based CCD on RHB adsorption, 0.015–0.035 g $Zn(OH)_2$ NPs-AC nanoparticles loaded on activated carbon were added into 50 mL RHB solutions with diverse pH and concentrations for a preset sonication time at 25°C. In order to study these factors, sonication time in the range of 2.0–6.0 min, initial concentration of RHB in the range of 5–35 mg L^{-1} and pH in the range of 2.0–10.0 were considered. In addition, each variable was chosen at five-level and R% of RHB dye as responses and outcomes are displayed in Table 1. To investigate about the highest adsorption of RHB, 0.025 g adsorbent with a concentration of 13.5 mg L^{-1} and pH of 4.0 was added to RHB solutions and shaken strongly at 25°C for 4 min. After employing centrifugal force at 3,000 rpm for 15 min, with the help of an UV-vis spectrophotometer (V-530, Jasco, Japan) at a wave length of 554 nm (maximum absorbance), the ultimate concentration of purpurin in the supernatant was verified. The percentage of RHB deletion (R%) and quantity of RHB adsorbed per unit mass of adsorbent q_e (mg g^{-1}) were procured employing the ensuing equations [32].

Table 2
Design matrix and the response

Run	X_1	X_2	X_3	X_4	$R\%_{RHB}$
1	20.000	6.0000	0.030000	2.0000	90.980
2	20.000	6.0000	0.030000	4.0000	95.300
3	20.000	6.0000	0.030000	4.0000	94.820
4	20.000	6.0000	0.030000	4.0000	98.420
5	27.500	8.0000	0.035000	3.0000	96.860
6	12.500	8.0000	0.035000	3.0000	98.250
7	20.000	6.0000	0.030000	4.0000	95.780
8	27.500	4.0000	0.035000	3.0000	80.160
9	27.500	4.0000	0.025000	3.0000	99.000
10	20.000	6.0000	0.020000	4.0000	95.000
11	20.000	6.0000	0.030000	4.0000	95.160
12	20.000	6.0000	0.030000	4.0000	100.00
13	27.500	8.0000	0.025000	3.0000	92.160
14	12.500	8.0000	0.035000	5.0000	99.780
15	20.000	6.0000	0.030000	4.0000	95.120
16	12.500	4.0000	0.025000	5.0000	93.640
17	27.500	8.0000	0.035000	5.0000	75.590
18	12.500	4.0000	0.025000	3.0000	100.00
19	12.500	8.0000	0.025000	5.0000	91.570
20	35.000	6.0000	0.030000	4.0000	90.500
21	27.500	4.0000	0.035000	5.0000	96.000
22	5.0000	6.0000	0.030000	4.0000	99.620
23	12.500	4.0000	0.035000	3.0000	98.960
24	20.000	6.0000	0.030000	6.0000	92.310
25	12.500	4.0000	0.035000	5.0000	95.410
26	12.500	8.0000	0.025000	3.0000	96.680
27	27.500	8.0000	0.025000	5.0000	92.110
28	27.500	4.0000	0.025000	5.0000	98.280
29	20.000	2.0000	0.030000	4.0000	100.00
30	20.000	10.000	0.030000	4.0000	98.000

Table 1
Process variables and their level for the RHB adsorption by CCD

Factors	Levels			Star point α = 2.0	
	Low (–1)	Central (0)	High (+1)	$-\alpha$	$+\alpha$
Initial RHB (X_1) concentration (mg L^{-1})	12.5	20	27.5	5	35
pH (X_2)	4.0	6.0	8.0	2.0	10.0
Adsorbent (g) (X_3)	0.025	0.03	0.035	0.02	0.04
Sonication time (min) (X_4)	3.0	4.0	5.0	2.0	6.0

2.5. Artificial neural network

From the field of ANN model, back propagation algorithm as the training algorithm for a feed-forward network has been applied. Initially, the model tried to compare the ultimate computed data for FFBP with the experimentally detected outcomes.

Next, after computation of the errors, they were propagated backwards and used for adjusting each neuron weight. The evaluation of input variables namely RHB concentrations, adsorbent amount, and contact time was performed all over the process. In that respect, 30 experimental points were utilized to feed the model. Data adjustment was resulted from training, test, and validation sets 60%, 20%, and 20% data points respectively. Based on the ensuing Eq. (1), the normalization of all of the data points were done in the range of [0.1, 0.9] due to the application of tan-sigmoidal transfer function [33]:

$$y = 0.8 \times \left(\frac{X - X_{\min}}{X_{\max} - X_{\min}} \right) + 0.1 \quad (1)$$

By assuming X in the above formula as a variable, then $X_{\min}$ is the minimum value and $X_{\max}$ is the maximum value.

3. Results and discussion

3.1. Model fitting and statistical analysis

To create a systematic number of experiments (30 runs) in five levels, CCD under RSM was employed. RSM made it feasible to model the experimental data nonlinearly [34–36]. Not only did the CCD avoid running unnecessary experiments but also was beneficial for realizing the synergies among the variables and supply value about interaction between the parameters.

$$\begin{aligned} R\%_{\mathrm{RHB}} = {} & 96.712 - 2.5246X_1 - 2.5988X_2 - 0.93542X_3 - 1.4471X_4 - \\ & 0.70958X_5 - 2.1219X_1X_2 - 0.88187X_1X_3 - 2.6731X_1X_4 + \\ & 0.015625X_1X_5 - 0.93687X_2X_3 - 2.7156X_2X_4 + 0.45562X_2X_5 + \\ & 1.1469X_3X_5 - 1.8819X_3X_5 + 0.29937X_4X_5 - 0.17364X_1^2 - \\ & 0.22239X_2^2 + 0.76261X_3^2 - 1.0061X_4^2 - 1.0761X_5^2 \end{aligned} \quad (2)$$

In the foregoing equation, the relative and positive values of each term are excellent indicators of their positive impact on response. On the other hands, their negative values demonstrate that the response after increasing their value is in decline. ANOVA (analysis of variance) was employed to assess the pivotal and efficient terms for modeling the response on the basis of *F*-test and *p*-values [37,38]. As the results are shown in (Table 3), the estimation of interaction impacts were easily carried out using ANOVA, while the estimation of factors impacts, Fisher's *F*-ratios and *p*-values were premised on sum of the squares. The effectiveness of this model for predicting the experimental data was proven by the "lack of fit *F*-value" of 1.601 and the corresponding *p*-value. The negligible value of lack of fit (more than 0.05) confirmed that the quadratic model was valid in explaining the experimental data of the current investigation [39]. In order to optimize the adsorption process, the profile for prognosticated values and desirability option (not demonstrated) was employed. Profiling the desirability of response involved stating the desirability function (DF) for $R\%_{\mathrm{RHB}}$ as dependent variable by determining the prognosticated $R\%_{\mathrm{RHB}}$ values. A scale in the range of disagreeable (0.0) to very agreeable (1.0) was employed for obtaining a comprehensive function which should be optimized through selecting the designed variables efficiently and enhancing the variables. Based on the CCD design matrix outcomes (Table 2), the max of $R\%_{\mathrm{RHB}}$ was 100.00% and the min of that was 75.59%. Concerning this range, the optimal condition at which the highest response can be attained was determined. The maximum restoration of 99.60% was acquired at optimum conditions regarding these estimations and desirability score of 1.0. For the factors including RHB concentration, pH, adsorbent dosage, and sonication time, the optimal values were estimated to be 13.5 mg L^{-1}, 0.025 g, and 4.0 min, respectively. By providing these conditions, 99.57% was predicted to be obtained for $R\%_{\mathrm{RHB}}$ with desirability of 1.0. Additionally, by doing three experiments at similar conditions, the validity of the predicted response at optimal conditions was inspected. Notably, the obtained experimental response was 99.40%, which was in excellent consistency with the prognosticated value.

3.2. Modeling of ultrasonic-supported deletion process by ANN

Three functions of net input, weight (training), and transfer (tansig) monitor and control the function of the network. Mean square error (MSE) of 0.0815 was detected at epoch numbers 7 for deletion of RHB dye. At this point training was stopped and weights have been frozen since the network underwent testing phase. In Fig. 2, for optimal ANN Model, the MSE against the number of epochs is displayed. A pause in the training after epoch numbers 7 for ultrasonic supported deletion of RHB dye was spotted. Also in Fig. 2, the diminution of the MSE throughout the training process is demonstrated. In addition, by referring to the plot of error histogram for adsorption process in Fig. 3, it is apparent that the errors in this deletion process are insignificant. In the course of the net training process in this study, the MSE premised on the function of error performance showed a minimum value at five neurons. A 4–5–1 the ANN model with four input layers (including initial RHB dye concentration, pH, ultrasonic time, and adsorbent dosage) and premised on the output layers (deletion of target compounds) was proved to be significantly reliable for predicting and reckoning the RHB deletion with MSE of 0.05292 for train, of 0.1894 for test, and of 0.0983 for validation. Also the correlation coefficient (R^2) of 0.9689, 0.9142, and 0.9701 was predicted and estimated for train, test, and validation, respectively, in ultrasonic supported deletion of RHB dye.

3.3. Response surface methodology

In Fig. 4, the 3D RSM surfaces of RHB dye deletion percentage against influential variables are demonstrated. In Figs. 4a and b, the interaction of pH with RHB concentration and sonication time is exhibited. It is shown that pH has a direct positive impact on the RHB deletion percentage since the percentage increased by raising the pH. This finding is explainable in this way that at low pH the adsorbent

Table 3
Results of ANOVA for the response surface quadratic model for *R*% of RHB

Source of variation	Df	RHB dye			
		Sum of square	Mean square	*F*-value	*p*-value
Model	14	896.43	44.821	18.878	<0.0001
X_1	1	162.08	162.08	68.265	<0.0001
X_2	1	21.000	21.000	8.8446	0.012655
X_3	1	50.257	50.257	21.167	0.000763
X_4	1	12.084	12.084	5.0895	0.045410
X_1X_2	1	14.044	14.044	5.9148	0.033289
X_1X_3	1	117.99	117.99	49.696	<0.0001
X_1X_4	1	3.3215	3.3215	1.3989	0.26184
X_2X_3	1	21.045	21.045	8.8636	0.012583
X_2X_4	1	56.663	56.663	23.865	0.000482
X_3X_4	1	1.4340	1.4340	0.60396	0.45346
X_1^2	1	1.4507	1.4507	0.61099	0.45091
X_2^2	1	17.060	17.060	7.1850	0.021389
X_3^2	1	29.694	29.694	12.506	0.004661
X_4^2	1	33.970	33.970	14.307	0.003034
Residual	11	26.118	2.37		
Lack of fit	6	17.177	2.86	1.6011	0.31103
Pure error	5	8.9405	1.788		
Correlation total	29	922.5			

1. Sum of squares
2. Degree freedom
3. Mean square

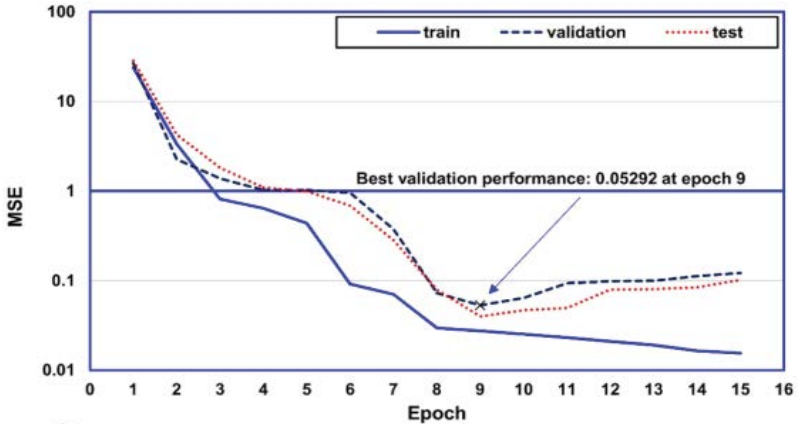

Fig. 2. Evolution of training, validation, and test errors as a function of the number of training epochs during ANN for the RHB removal by $Zn(OH)_2$-NPs-AC.

surfaces get positive charge because of the AC functional groups protonation. Thus, intense repulsive forces between the adsorbent and cationic dye molecules can diminish the RHB deletion percentage. Deprotonation of the AC adsorption sites occurs upon any increase in the initial pH and as a result, the OH and COOH adsorb the RHB molecule via electrostatic interaction and/or hydrogen bonding. In Fig. 4c, the relationship of initial dye concentration and adsorbent dosage as well as their influence on the deletion percentage is shown. It became apparent that the deletion percentage of RHB dye reduced at higher initial dye concentration which was relative to the increase in the ratio of dye molecules to the available adsorption surface area.

3.4. Adsorption equilibrium

The experimental adsorption equilibrium data were evaluated and distinct models of Freundlich, Dubinin–Radushkevich, Temkin, and Langmuir isotherms [40–42] in their conventional linear form were employed for considering

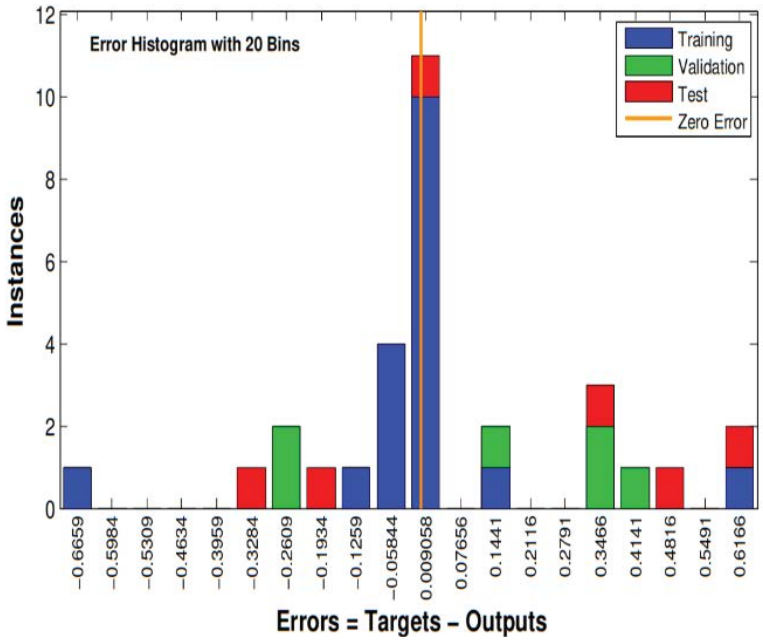

Fig. 3. Plot of error histogram for the removal process.

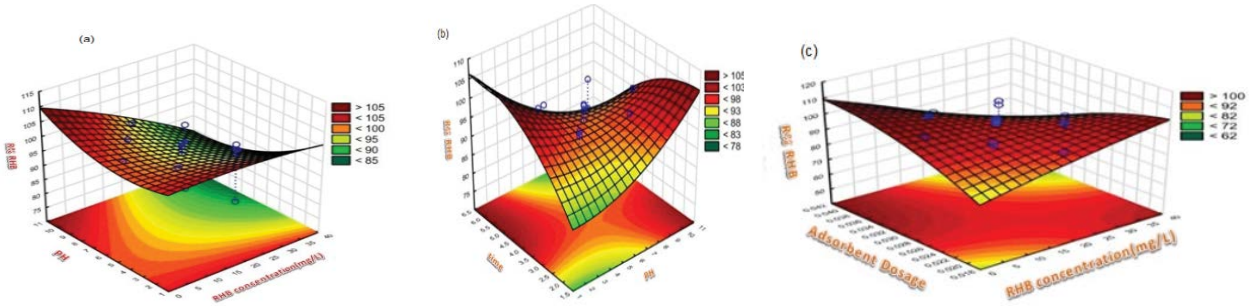

Fig. 4. Response surfaces for the CCD: (a) pH-RHB concentration, (b) pH-time, and (c) adsorbent dosage–DSB concentration.

Table 4
Various isotherm constants and their coefficient of determination calculated for the adsorption of RHB on $Zn(OH)_2$NPs-AC

Isotherm	Equation	Parameters	Value of parameters for RHB (0.025 g)
Langmuir	$q_e = q_m bC_e/(1 + bC_e)$	q_m (mg g^{-1})	76.38
		K_a (L mg^{-1})	0.240
		R^2	0.998
Freundlich	$\ln q_e = \ln K_F + (1/n) \ln C_e$	$1/n$	0.681
		K_F (L mg^{-1})	3.251
		R^2	0.98
Tempkin	$q_e = B_1 \ln K_T + B_1 \ln C_e$	B_1	16.179
		K_T (L mg^{-1})	2.413
		R^2	0.978
Dubinin–Radushkevich (D–R)	$\ln q_e = \ln Q_s - B\varepsilon^2$	Q_s (mg g^{-1})	37.33
		$B \times 10^{-7}$	–2
		E (kJ mol^{-1})	1,582.278
		R^2	0.973

the mechanism of RHB dye adsorption onto $Zn(OH)_2$-NPs-AC. Thereafter, their relative constants were estimated from the slopes and intercepts of respective lines (Table 4). The models were employed while the dosages of the adsorbent and other variables were maintained at optimal conditions (Table 4). After adjusting the experimental data to the isotherm models, the greater values of the coefficient of determination (R^2 = 0.998) was obtained. It became apparent that the RHB dye adsorption onto $Zn(OH)_2$-NPs-AC was excellently described by the Langmuir isotherm. The model could quantitatively describe the creation of a monolayer of adsorbate on the outer surface of the $Zn(OH)_2$-NPs-AC. Also, the equilibrium distribution of RHB dye between the solid and liquid phase was clearly shown in this model.

3.5. Adsorption kinetics

Numerous parameters pertain to the physicochemical factors that sorption is taking place under and the state of the solid can control the kinetics of reactions in the adsorption process. A close examination was performed on some kinetic models including Elovich, pseudo-first-order, pseudo-second-order, and intraparticle diffusion models to consider the sorption process of RHB dye onto the adsorbent [40,41,43]. Considering the plots of the kinetic model equations, identical parameters were estimated (Table 5). The criterion for applicability of models was premised on deciding the respective correlation coefficient (R^2) and conformity between calculated and experimental values of q_e. Pseudo-second-order kinetic model provided us with not only the highest values of R^2 = 0.998 for RHB dye but also with excellent conformity between two q_e values. Also limiting steps in this model might prove that the process is a kind of chemisorption process.

4. Conclusion

The influence of important variables like initial RHB dye concentration, pH, sonication time, and adsorbent dosage on the effectiveness of the deletion process was examined closely by CCD. The application of ANN model for developing an empirical model was fruitful and the findings put the ANN model in a list of successful tools in predicting under study dye adsorption of $Zn(OH)_2$-NPs-AC. Langmuir model in comparison with other investigated isotherm models for the adsorption process was proven to be successful in describing the equilibrium data. In addition, the kinetic models to describe experimental data points at various initial concentrations of adsorbate show that can be successfully fitted to the pseudo-second-order kinetic model. The optimized method was successfully applied to real wastewater samples. Moreover, the findings of the present study can assist the researchers and industries to take advantage of ultrasound devices in dye adsorption more efficiently. It is noteworthy that the application of an optimized method for real wastewater samples provided positive results.

Table 5
Kinetic parameters for the adsorption of RHB on $Zn(OH)_2$ NPs-AC

Model	Parameters	Value of parameters for RHB
Pseudo-first-order kinetic	k_1 (min^{-1})	0.677
	q_e (calc) (mg g^{-1})	9.183
	R^2	0.972
Pseudo-second-order kinetic	k_2 (min^{-1})	0.124
	q_e (calc) (mg g^{-1})	45.45
	R^2	0.999
Intraparticle diffusion	K_{diff} (mg g^{-1} min$^{-1/2}$)	3.72
	C (mg g^{-1})	35.07
	R^2	0.974
Elovich	β (g mg^{-1})	0.375
	α (mg g^{-1} min^{-1})	65
	R^2	0.972

Acknowledgment

The authors gratefully acknowledge the financial support from the Payame Noor University, Branch of Busher, Iran.

References

[1] E. Baldikova, M. Safarikova, I. Safarik, Organic dyes removal using magnetically modified rye straw, J. Magn. Magn. Mater., 380 (2015) 181–185.
[2] V. Rocher, J.-M. Siaugue, V. Cabuil, A. Bee, Removal of organic dyes by magnetic alginate beads, Water Res., 42 (2008) 1290–1298.
[3] Y.E. Unsal, M. Soylak, M. Tuzen, Dispersive liquid–liquid microextraction–spectrophotometry combination for determination of rhodamine B in food, water, and environmental samples, Desal. Water Treat., 55 (2015) 2103–2108.
[4] M.R. Parvizi, N. Karachi, Isotherm and kinetic study of Disulfin Blue and Methyle Orange dyes by adsorption onto by titanium dioxide-NPs loaded onto activated carbon: experimental design, Orient. J. Chem., 33 (2017) 2559–2565.
[5] V.V. Pathak, R. Kothari, A.K. Chopra, D.P. Singh, Experimental and kinetic studies for phycoremediation and dye removal by *Chlorella pyrenoidosa* from textile wastewater, J. Environ. Manage., 163 (2015) 270–277.
[6] M. Arshadi, A.R. Faraji, M. Mehravar, Dye removal from aqueous solution by cobalt nano particles decorated aluminum silicate: kinetic, thermodynamic and mechanism studies, J. Colloid Interface Sci., 440 (2015) 91–101.
[7] T.A. Khan, S. Sharma, I. Ali, Adsorption of Rhodamine B dye from aqueous solution onto acid activated mango (*Magnifera indica*) leaf powder: equilibrium, kinetic and thermodynamic studies, J. Toxicol. Environ. Health Sci., 3 (2011) 286–297.
[8] X. Huang, X. Bo, Y. Zhao, B. Gao, Y. Wang, S. Sun, Q. Yue, Q. Li, Effects of compound bioflocculant on coagulation performance and floc properties for dye removal, Bioresour. Technol. 165 (2014) 116–121.
[9] C.K. Araujo, G.R. Oliveira, N.S. Fernandes, C.L. Zanta, S.S. Castro, D.R. da Silva, C.A. Martinez-Huitle, Electrochemical removal of synthetic textile dyes from aqueous solutions using Ti/Pt anode: role of dye structure, Environ. Sci. Pollut. Res. Int., 21 (2014) 9777–9784.
[10] A. Asfaram, M. Ghaedi, G.R. Ghezelbash, F. Pepe, Application of experimental design and derivative spectrophotometry methods in optimization and analysis of biosorption of binary mixtures of basic dyes from aqueous solutions, Ecotoxicol. Environ. Saf., 139 (2017) 219–227.
[11] N. Harruddin, N. Othman, A.L. Ee Sin, R.N. Raja Sulaiman, Selective removal and recovery of Black B reactive dye from

simulated textile wastewater using the supported liquid membrane process, Environ. Technol., 36 (2015) 271–280.
[12] M.A. Khan, M. Siddique, F. Wahid, R. Khan, Removal of reactive blue 19 dye by sono, photo and sonophotocatalytic oxidation using visible light, Ultrason. Sonochem., 26 (2015) 370–377.
[13] H. Sun, X. Yang, L. Zhao, Y. Li, J. Zhang, L. Tang, Y. Zou, C. Dong, J. Lian, Q. Jiang, Nanostructured Co_xNi_{1-x} bimetallic alloys for high efficient and ultrafast adsorption: experiments and first-principles calculations, RSC Adv., 6 (2016) 9209–9220.
[14] H.Z. Khafri, M. Ghaedi, A. Asfaram, M. Safarpoor, Synthesis and characterization of ZnS:Ni-NPs loaded on AC derived from apple tree wood and their applicability for the ultrasound assisted comparative adsorption of cationic dyes based on the experimental design, Ultrason. Sonochem., 38 (2017) 371–380.
[15] S. Dhananasekaran, R. Palanivel, S. Pappu, Adsorption of methylene blue, bromophenol blue, and Coomassie brilliant blue by α-chitin nanoparticles, J. Adv. Res., 7 (2016) 113–124.
[16] A. Asfaram, M. Ghaedi, A. Goudarzi, Optimization of ultrasound-assisted dispersive solid-phase microextraction based on nanoparticles followed by spectrophotometry for the simultaneous determination of dyes using experimental design, Ultrason. Sonochem., 32 (2016) 407–417.
[17] M. Arabi, M. Ghaedi, A. Ostovan, J. Tashkhourian, H. Asadallahzadeh, Synthesis and application of molecularly imprinted nanoparticles combined ultrasonic assisted for highly selective solid phase extraction trace amount of celecoxib from human plasma samples using design expert (DXB) software, Ultrason. Sonochem., 33 (2016) 67–76.
[18] S. Bahrani, M. Ghaedi, M.J.K. Mansoorkhani, A. Asfaram, A.A. Bazrafshan, M.K. Purkait, Ultrasonic assisted dispersive solid-phase microextraction of Eriochrome Cyanine R from water sample on ultrasonically synthesized lead(II) dioxide nanoparticles loaded on activated carbon: experimental design methodology, Ultrason. Sonochem., 34 (2017) 317–324.
[19] P. Nasehi, M. Saei Moghaddam, S.F. Abbaspour, N. Karachi, Preparation and characterization of a novel Mn-Fe_2O_4 nanoparticle loaded on activated carbon adsorbent for kinetic, thermodynamic and isotherm surveys of aluminum ion adsorption, Sep. Sci. Technol., 55 (2019) 1078–1088.
[20] A.B. Aghaie, M.R. Hadjmohammadi, Fe_3O_4@p-Naphtholbenzein as a novel nano sorbent for highly effective removal and recovery of Berberine: response surface methodology for optimization of ultrasound assisted dispersive magnetic solid phase extraction, Talanta, 156–157 (2016) 18–28.
[21] M. Arabi, M. Ghaedi, A. Ostovan, Development of a lower toxic approach based on green synthesis of water-compatible molecularly imprinted nanoparticles for the extraction of hydrochlorothiazide from human urine, ACS Sustainable Chem. Eng., 5 (2017) 3775–3785.
[22] E.A. Dil, M. Ghaedi, A. Asfaram, F. Mehrabi, A.A. Bazrafshan, A.M. Ghaedi, Trace determination of safranin O dye using ultrasound assisted dispersive solid-phase micro extraction: artificial neural network-genetic algorithm and response surface methodology, Ultrason. Sonochem., 33 (2016) 129–140.
[23] M. Ghazaghi, H. Shirkhanloo, H.Z. Mousavi, A.M. Rashidi, Ultrasound-assisted dispersive solid phase extraction of cadmium(II) and lead(II) using a hybrid nanoadsorbent composed of graphene and the zeolite clinoptilolite, Microchim. Acta, 182 (2015) 1263–1272.
[24] S.V. Pakhale, S.S. Bhagwat, Purification of serratiopeptidase from *Serratia marcescens* NRRL B 23112 using ultrasound assisted three phase partitioning, Ultrason. Sonochem., 31 (2016) 532–538.
[25] A. Asfaram, M. Ghaedi, K. Dashtian, Rapid ultrasound-assisted magnetic microextraction of gallic acid from urine, plasma and water samples by HKUST-1-MOFFe_3O_4-GA-MIP-NPs: UV–vis detection and optimization study, Ultrason. Sonochem., 34 (2017) 561–570.
[26] A. Asfaram, M. Ghaedi, M.K. Purkait, Novel synthesis of nanocomposite for the extraction of Sildenafil Citrate (*Viagra*) from water and urine samples: process screening and optimization, Ultrason. Sonochem., 38 (2017) 463–472.
[27] H. Shirkhanloo, M. Falahnejad, H.Z. Mousavi, On-line ultrasound-assisted dispersive micro-solid-phase extraction based on amino bimodal mesoporous silica nanoparticles for the preconcentration and determination of cadmium in human biological samples, Biol. Trace Elem. Res., 171 (2016) 472–481.
[28] F. Mehrabi, A. Vafaei, M. Ghaedi, A.M. Ghaedi, E. Alipanahpour Dil, A. Asfaram, Ultrasound assisted extraction of Maxilon Red GRL dye from water samples using cobalt ferrite nanoparticles loaded on activated carbon as sorbent: optimization and modeling, Ultrason. Sonochem., 38 (2017) 672–680.
[29] M. Ghaedi, G. Negintaji, F. Marahel, Solid phase extraction and removal of brilliant green dye on zinc oxide nanoparticles loaded on activated carbon: new kinetic model and thermodynamic evaluation, J. Ind. Eng. Chem., 20 (2014) 1444–1452.
[30] P.S. Ardekani, H. Karimi, M. Ghaedi, A. Asfaram, M.K. Purkait, Ultrasonic assisted removal of methylene blue on ultrasonically synthesized zinc hydroxide nanoparticles on activated carbon prepared from wood of cherry tree: experimental design methodology and artificial neural network, J. Mol. Liq., 229 (2017) 114–124.
[31] A. Asfaram, M. Ghaedi, S. Hajati, A. Goudarzi, A.A. Bazrafshan, Simultaneous ultrasound-assisted ternary adsorption of dyes onto copper-doped zinc sulfide nanoparticles loaded on activated carbon: optimization by response surface methodology, Spectrochim. Acta, Part A, 145 (2015) 203–212.
[32] M. Kiania, S.Bagheri, N. Karachi, E. Alipanahpour Dil, Adsorption of purpurin dye from industrial wastewater using Mn-doped Fe_2O_4 nanoparticles loaded on activated carbon, Desal. Water Treat., 152 (2019) 366–373.
[33] A. Asfaram, M. Ghaedi, S. Hajati, A. Goudarzi, Synthesis of magnetic γ-Fe_2O_3-based nanomaterial for ultrasonic assisted dyes adsorption: modeling and optimization, Ultrason. Sonochem., 32 (2016) 418–431.
[34] P. Saravanan, J.-H. Hsu, D. Sivaprahasam, S. Kamat, Structural and magnetic properties of γ-Fe_2O_3 nanostructured compacts processed by spark plasma sintering, J. Magn. Magn. Mater., 346 (2013) 175–177.
[35] E.A. Dil, M. Ghaedi, A. Ghaedi, A. Asfaram, M. Jamshidi, M.K. Purkait, Application of artificial neural network and response surface methodology for the removal of crystal violet by zinc oxide nanorods loaded on activate carbon: kinetics and equilibrium study, J. Taiwan Inst. Chem. Eng., 59 (2016) 210–220.
[36] M. Ghaedi, M. Shahamiri, S. Hajati, B. Mirtamizdoust, A novel PVC-membrane optical sensor for high sensitive and selective determination of Cu2+ ion based on synthesized (E)-N′-(pyridin-2-ylmethylene)isonicotin-ohydrazide, J. Mol. Liq., 199 (2014) 483–488.
[37] S. Karimifard, M.R. Alavi Moghaddam, Enhancing the adsorption performance of carbon nanotubes with a multistep functionalization method: optimization of Reactive Blue 19 removal through response surface methodology, Process Saf. Environ. Prot., 99 (2016) 20–29.
[38] S.L. Lee, S.W. Liew, S.T. Ong, Experimental design approach for methylene blue dye removal in aqueous environment by nitrilotriacetic modified banana pith, Acta Chim. Slov., 63 (2016) 144–153.
[39] S.-Y. Jeong, J.-W. Lee, Optimization of pretreatment condition for ethanol production from oxalic acid pretreated biomass by response surface methodology, Ind. Crop. Prod., 79 (2016) 1–6.
[40] M. Ghaedi, A. Hassanzadeh, S.N. Kokhdan, Multiwalled carbon nanotubes as adsorbents for the kinetic and equilibrium study of the removal of Alizarin Red S and Morin, J. Chem. Eng. Data, 56 (2011) 2511–2520.
[41] M. Ghaedi, B. Sadeghian, A.A. Pebdani, R. Sahraei, A. Daneshfar, C. Duran, Kinetics, thermodynamics and equilibrium evaluation of direct yellow 12 removal by adsorption onto silver nanoparticles loaded activated carbon, Chem. Eng. J., 187 (2012) 133–141.
[42] S. Hajati, M. Ghaedi, B. Barazesh, F. Karimi, R. Sahraei, A. Daneshfar, A. Asghari, Application of high order derivative spectrophotometry to resolve the spectra overlap between BG and MB for the simultaneous determination of them: ruthenium nanoparticle, J. Ind. Eng. Chem., 20 (2014) 2421–2427.
[43] M. Toor, B. Jin, Adsorption characteristics, isotherm, kinetics, and diffusion of modified natural bentonite for removing diazo dye, Chem. Eng. J., 187 (2012) 79–88.

Supplementry information

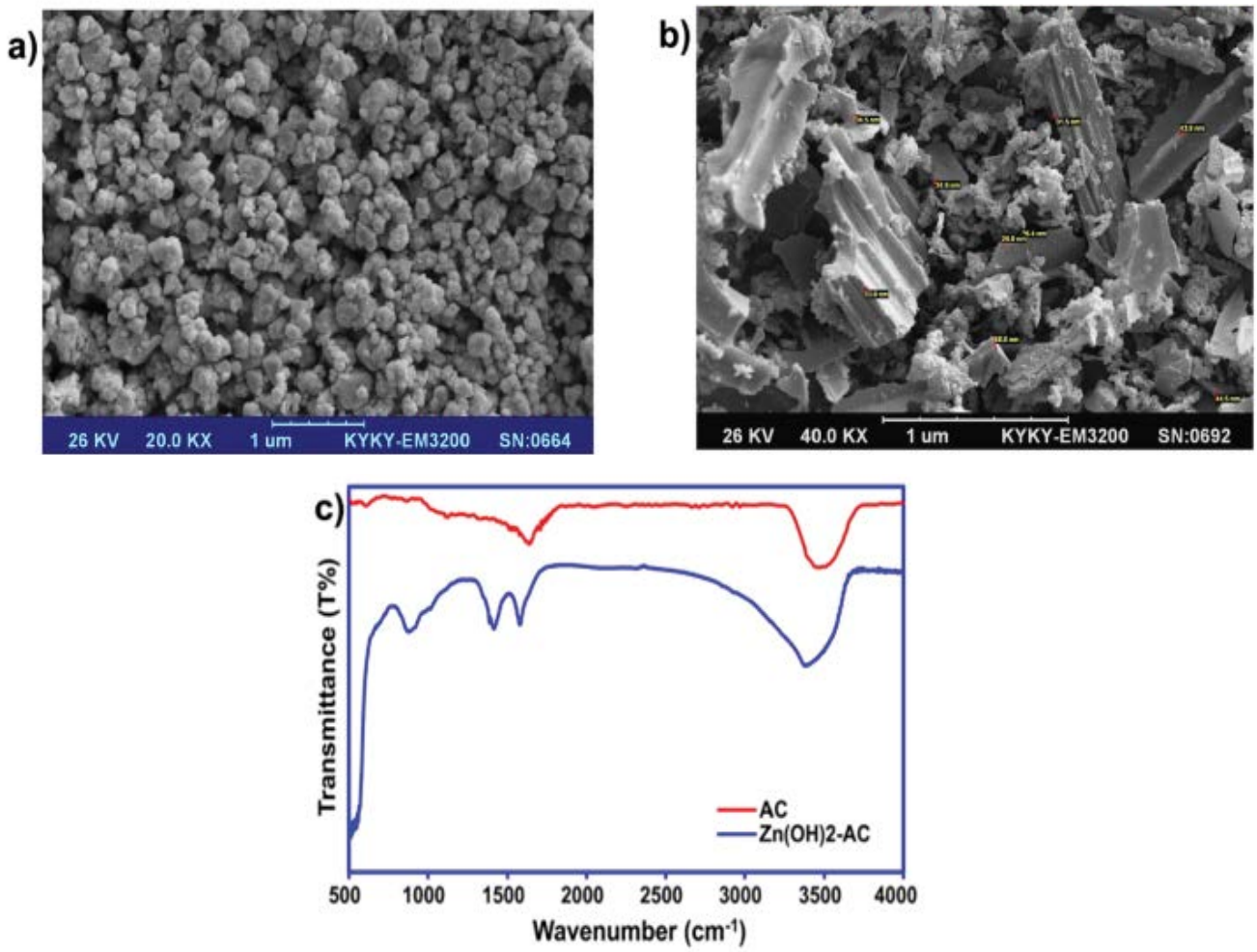

Fig. 1. (a) FESEM images of the Zn $(OH)_2$-NPs (the average size of NP: 60 nm), (b) $Zn(OH)_2$-NPs-AC, and (c) FT-IR of the prepared AC and $Zn(OH)_2$-NPs-AC.

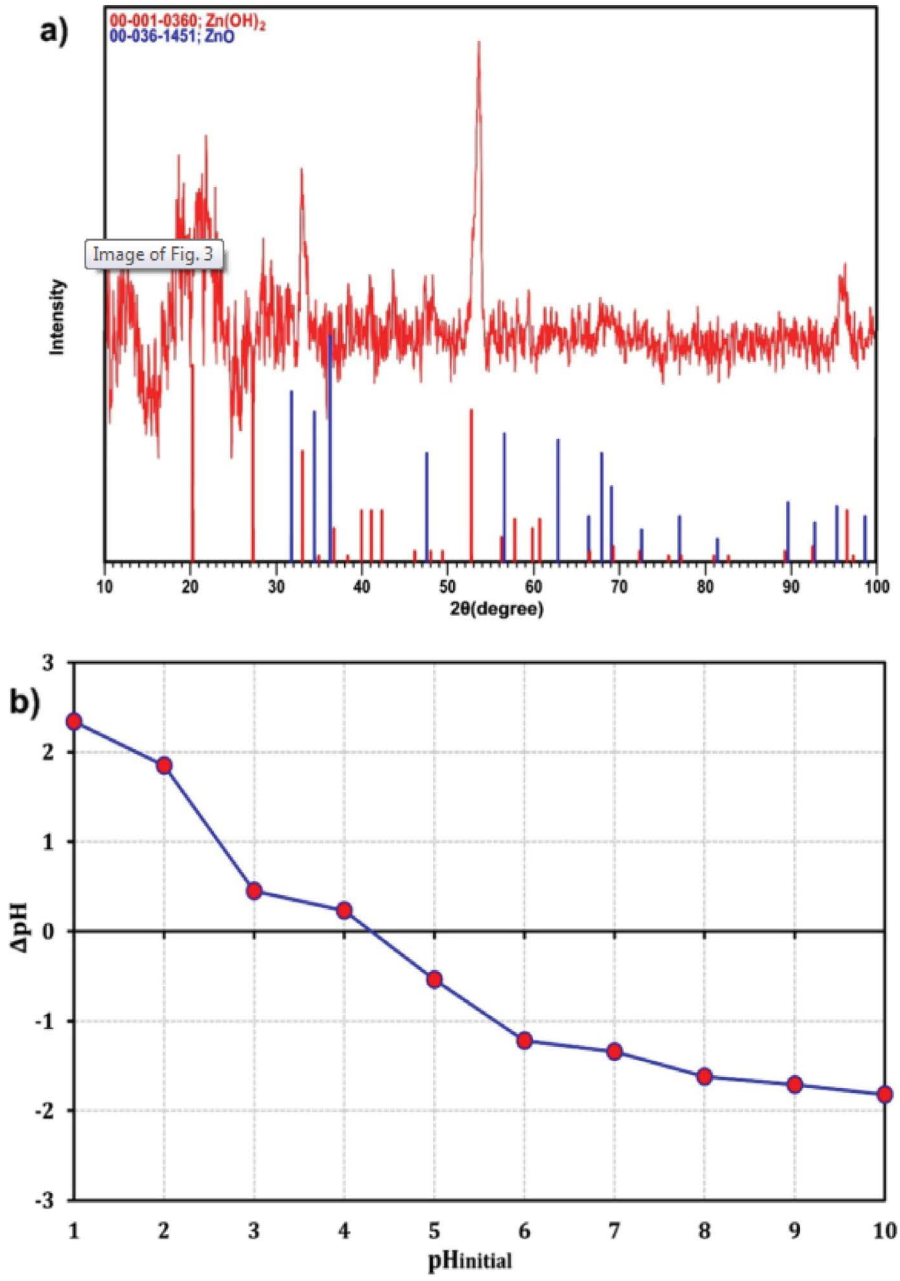

Fig. 2. (a) XRD pattern and $Zn(OH)_2$-NPs-AC and (b) pH_{PZC} values of $Zn(OH)_2$-NPs-AC (*V*: 50 mL; KNO_3: 0.1 mol L^{-1}; $Zn(OH)_2$-NPs-AC; 0.1 g; stirred time: 24 h; room temperature).